Anomalous Pressure Dependence of the Charge Density Wave and Fermi Surface Reconstruction in $BaFe_2Al_9$

Mahmoud Abdel-Hafiez,[1,2,*] Muthukumaran Sundaramoorthy,[3,4] Nabeel M. Jasim,[1] K. A. Irshad,[4] Chia Nung Kuo,[5,6] Chin Shan Lue,[5,6] F. L. Carstens,[7] A. Bertrand,[8] M. Mito,[8] Rüdiger Klingeler,[7] Vladislav Borisov,[9,10] Anna Delin,[11,12] Boby Joseph,[4] Olle Eriksson,[9,10] Sonachalam Arumugam,[3,13,†] and Govindaraj Lingannan[3,4,14,‡]

[1]*Department of Applied Physics and Astronomy, University of Sharjah, P.O. Box 27272 Sharjah, United Arab Emirates*
[2]*Department of Physics, Faculty of Science, Fayoum University, Fayoum 63514, Egypt*
[3]*Centre for High Pressure Research, School of Physics, Bharathidasan University, Tiruchirappalli 620024, India*
[4]*Elettra-Sincrotrone Trieste S.C.p.A., S.S. 14, Km 163.5 in Area Science Park, Basovizza 34149, Italy*
[5]*Department of Physics, National Cheng Kung University, Tainan 70101, Taiwan*
[6]*Taiwan Consortium of Emergent Crystalline Materials, National Science and Technology Council, Taipei 10601, Taiwan*
[7]*Kirchhoff Institute for Physics, Heidelberg University, INF 227, D-69120 Heidelberg, Germany*
[8]*Graduate School of Engineering, Kyushu Institute of Technology, Fukuoka 804-8550, Japan*
[9]*Department of Physics and Astronomy, Uppsala University, Uppsala, 751 20, Sweden*
[10]*Wallenberg Initiative Materials Science for Sustainability (WISE), Uppsala University, Uppsala, 751 20, Sweden*
[11]*Department of Applied Physics, KTH Royal Institute of Technology, 516, SE-75121, Stockholm, Sweden*
[12]*Swedish e-Science Research Center (SeRC), KTH Royal Institute of Technology, SE-10044, Stockholm, Sweden*
[13]*Tamil Nadu Open University, Chennai 600015, India*
[14]*College of General Education, University of Doha for Science and Technology, Qatar, Doha, Qatar*

(Received 7 August 2025; revised 16 September 2025; accepted 6 November 2025; published 2 December 2025)

We investigate the pressure evolution of charge density wave (CDW) order in the intermetallic compound $BaFe_2Al_9$, which undergoes a pronounced first-order CDW transition ∼112 K at ambient pressure. High-pressure electrical resistivity and magnetization measurements reveal a systematic enhancement of the CDW transition temperature (T_{CDW}) at a rate of ∼60 K/GPa, reaching 300 K under ∼3.2 GPa. The transition sharpness diminishes with pressure, indicating a crossover from first- to second-order behavior. Fermi liquid (FL) fits to the low-temperature resistivity reveal an increase in residual resistivity and a nonmonotonic evolution of the FL coefficient, indicating a pressure-induced Fermi surface (FS) reconstruction. Synchrotron x-ray diffraction reveals anisotropic lattice compression, a change in the compression trend of lattice parameters, and an abrupt change in microstrain at ∼3.6 GPa. Density functional theory calculations reveal pressure-induced flattening of quasi-two-dimensional FS sheets associated with the CDW nesting vector, consistent with enhanced nesting. These findings highlight the critical role of lattice strain and electronic structure evolution in stabilizing a high-temperature CDW phase, making $BaFe_2Al_9$ a rare example of a three-dimensional material where pressure promotes rather than suppresses the CDW order.

DOI: 10.1103/dxzf-fx8k

Charge density waves (CDWs) are collective electronic states characterized by a periodic modulation of the conduction electron density, typically coupled to a corresponding lattice distortion. They often arise in low-dimensional materials, where enhanced Fermi surface (FS) nesting allows electronic instabilities to lower the system's total energy. However, recent discoveries have identified the CDW order in several three-dimensional (3D) intermetallic systems, including the rare-earth tritellurides, ternary antimonides, and ternary germanides [1–3]. These systems offer a broader landscape to study conventional CDW mechanisms and explore how electronic and structural degrees of freedom couple under external stimuli. The intermetallic $BaFe_2Al_9$ exhibits a sharp CDW transition ∼112 K, which manifests as a large resistivity drop and a magnetic anomaly. It crystallizes in a $P6/mmm$ hexagonal structure characterized by Fe-centered Al polyhedra that form interconnected triangular networks within the a-b plane (see Fig. S1

*Contact author: mahmoudhafiez@gmail.com
†Contact author: sarumugam1963@yahoo.com
‡Contact author: lgovindphy@gmail.com

in Supplemental Material [4]). A previous study has indicated that the CDW transition in $BaFe_2Al_9$ is incommensurate and first order [5]. The primary signatures of this arise from the temperature-dependent anisotropic lattice compression and anomalies in thermal expansion. These observations suggest a strong coupling between the electronic instabilities and the lattice strain [5,6]. Interestingly, the isostructural Co analog $BaCo_2Al_9$ and $SrCo_2Al_9$ do not exhibit CDW order and remain metallic across the same temperature range, highlighting the crucial role of Fe 3*d* electrons in driving the electronic instability [6,7]. Furthermore, while the CDW transition is typically suppressed under pressure due to a weakened FS nesting [2,3], $BaFe_2Al_9$ displays the opposite behavior, making it a rare example of pressure-enhanced CDW physics. Other two currently known examples are the cases of 1*T*-VSe_2 [8] and FeGe [9]. In 1*T*-VSe_2, the pressure-enhanced CDW is linked to the out-of-plane FS nesting and the CDW gap, and a CDW state at ambient temperature is achieved above 10 GPa [8]. In FeGe, a possible CDW state at ambient temperature emerges above 20 GPa, where the emergent CDW is assumed to be driven by the delicate balance between magnetic energy savings and Ge dimerization structural energy costs [9]. Given this background, $BaFe_2Al_9$ offers a valuable platform to explore how CDW transitions evolve under external pressure and how the FS and lattice strain interplay to stabilize the collective ground states. To this end, we conducted a comprehensive investigation combining high-pressure (HP) resistivity, magnetization, and synchrotron powder x-ray diffraction (PXRD) measurements up to 7 GPa. We further supported our experimental findings with density functional theory (DFT) calculations using realistic pressure-dependent structural inputs. We find that pressure systematically enhances the CDW transition temperature (T_{CDW}), driving it from 112 K at ambient pressure to nearly 260 K at 2.5 GPa, thus indicating the possibility of obtaining the CDW transition at ambient temperatures for a low pressure of ~3.2 GPa. Concurrently, the resistivity anomaly broadens, suggesting a change in the transition character from first to second order. Magnetization measurements also support this trend. Synchrotron HP PXRD reveals anisotropic lattice contraction and a distinct change in microstrain ~3.64 GPa, with a lattice parameter compression trend change. DFT calculations show significant flattening of quasi-two-dimensional FS sheets under pressure, leading to enhanced nesting. These results reveal a compelling scenario where microstrain and FS evolution under pressure work in tandem to stabilize and strengthen the CDW order. Our findings advance the understanding of strain-coupled electronic instabilities in 3D intermetallics and suggest the potential for tuning such phenomena in other systems.

Single crystals of $BaFe_2Al_9$ were grown using the aluminum self-flux method, with detailed synthesis procedures available in Ref. [6]. Electrical transport measurements were performed using a closed cycle refrigerator system, covering the temperature range of 4 to 300 K during warming. Resistivity measurements under hydrostatic pressure (up to 3 GPa) were performed using a clamp-type hybrid double-cylinder piston pressure cell; preparation details are provided in Ref. [10]. Magnetic measurements were performed using a Quantum Design MPMS superconducting quantum interference device magnetometer. For the HP magnetization studies, a nonmagnetic BeCu piston-cylinder pressure cell was employed. All magnetization measurements were conducted under an applied magnetic field of 1 T [11]. Static magnetic susceptibility measurements were performed under an applied magnetic field of 0.1 T. HP synchrotron PXRD measurements were conducted at the Xpress beamline, Elettra-Sincrotrone Trieste, using monochromatic x-rays ($\lambda = 0.4957$ Å) [12]. Diffraction ring images collected with the Pilatus3S 6M large-area detector were converted into 2θ intensity plots using Dioptas software. To extract the instrumental parameters, the beamline setup was calibrated with a standard CeO_2 reference sample (SRM674b, National Institute of Standards and Technology). Structural refinement was carried out using the Rietveld method implemented in GSAS-II [13]. We performed the electronic structure calculations using the full-potential linear muffin-tin orbital method in RSPt software [14,15], employing DFT with the Perdew-Burke-Ernzerhof generalized-gradient approximation. Dynamical correlations were not included. We used a $(10 \times 20 \times 10)$ *k*-mesh for the Brillouin zone integration, and the Fermi surfaces were computed on a finer $(30 \times 60 \times 30)$ mesh. The calculations were based on experimentally determined lattice parameters at different pressures, with Al atomic positions fixed to their ambient-pressure values. For comparison, fully relaxed structures were also considered, as discussed later.

Figure 1 presents the temperature-dependent electrical resistivity [$\rho(T)$] of the $BaFe_2Al_9$ single crystal under various applied pressures. At ambient pressure, a distinct resistivity drop is observed near 112 K, marking the CDW transition temperature, as also shown in Fig. S2(a) of Supplemental Material [4]. The value of T_{CDW} was determined by taking the first derivative of the resistivity with respect to the temperature ($d\rho/dT$) shown in Fig. S2 (b) of Supplemental Material [4]. The relative resistivity change at the transition calculated using the relation $\Delta\rho/\rho(T_{CDW})$ yields approximately 67%, consistent with previously reported values (Refs. [5,6]). At ambient conditions, the resistivity displays metallic behavior down to ~110 K, followed by a sharp drop due to the onset of CDW order. Above T_{CDW}, the resistivity exhibits a linear temperature dependence attributed primarily to electron-phonon scattering, as indicated by the green guideline fits in Fig. 1. Upon applying pressure, T_{CDW} systematically shifts to higher temperatures, with an estimated positive pressure coefficient of $dT_{CDW}/dP \approx 60$ K/GPa. As summarized in Table S1 of Supplemental Material [4], this is the largest positive pressure coefficient ever reported for a

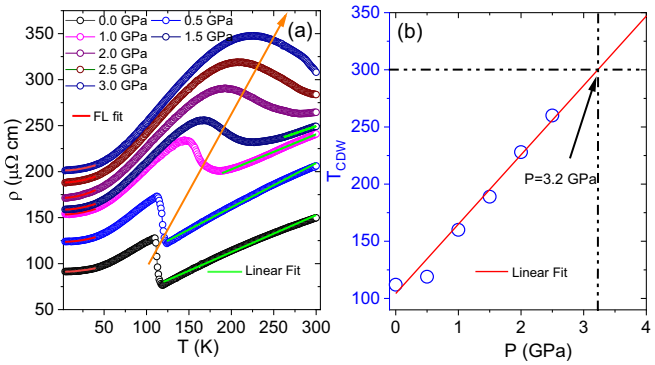

FIG. 1. (a) $\rho(T)$ measurements under various hydrostatic pressures. (b) T_{CDW} as a function of the pressure.

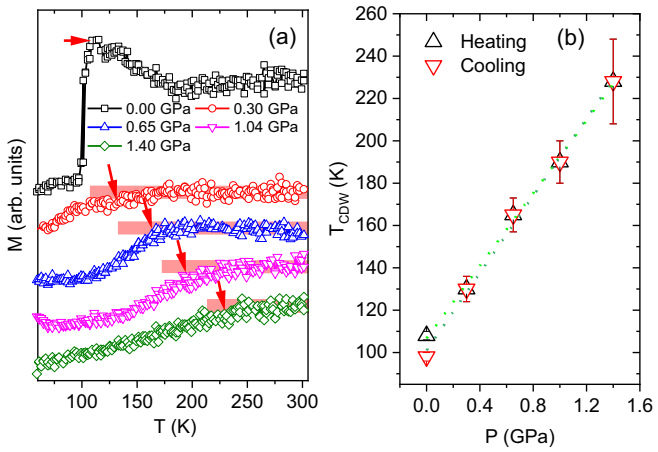

FIG. 2. (a) $M(T)$ under various fixed pressures measured during the heating process. (b) Pressure dependence of T_{CDW} extracted from both cooling and heating measurements. The dotted line is included as a guide to the eye to emphasize the overall trend of T_{CDW} with pressure.

CDW material, exceeding even strongly pressure-enhanced systems such as $TaSe_3$ (~46 K/GPa) [16], $1T$-VSe_2 (~18 K/GPa) [8], $SmNiC_2$ (~15 K/GPa) [17], and FeGe (~4 K/GPa) [9]. This extraordinary enhancement, in sharp contrast to the more common suppression of CDW order under compression, highlights a unique strain-coupled mechanism in $BaFe_2Al_9$ and underscores its broader relevance for understanding pressure-stabilized electronic orders in intermetallic systems. T_{CDW} values extracted from the $d\rho/dT$ analysis at each pressure are summarized in Fig. S3(a) of Supplemental Material [4]. As pressure increases, the CDW transition becomes more gradual, reflecting a crossover from a sharp, first-order- to a broadened, second-order-like transition [18]. This broadening indicates a possible change in the underlying transition mechanism [see Supplemental Material Fig. S3(b) [4]]. Figure 1(b) shows that T_{CDW} increases linearly with pressure up to 2.5 GPa. Note that the T_{CDW} value for 3 GPa is absent in Fig. 1(b), as we could not perform well the $d\rho/dT$ analysis due the availability of the $\rho(T)$ data only up to 300 K. A linear extrapolation suggests that T_{CDW} reaches 300 K at around 3.2 GPa.

To further explore the low-temperature electronic behavior, we fitted the resistivity curves using the Fermi liquid (FL) model: $\rho(T) = \rho_0 + AT^2$, where ρ_0 is the residual resistivity, and A is the FL coefficient, which reflects the electron-electron scattering strength. As shown by the red lines in Fig. 1. the fits are valid in the temperature range of 4 to 40 K, and the extracted fitting parameters are summarized in Table S2 of Supplemental Material [4]. The Kadowaki-Woods (KW) ratio given by A/γ_e^2 was calculated to assess the correlation strength. Here, A is the FL coefficient obtained from the fit, and γ_e is the Sommerfeld coefficient of the electronic specific heat ($\gamma_{\mathrm{e}} = 19.4\ \mathrm{mJ\,mol^{-1}\,K^{-2}}$ from Ref. [5]). Our A/γ_e^2 values increase with pressure and remain close to the universal KW value, indicating that $BaFe_2Al_9$ behaves as a strongly correlated Fermi liquid within the studied pressure range [19]. The pressure dependence of ρ_0 shows two distinct trends: a moderate increase below 1 GPa, followed by a more pronounced rise above 1.5 GPa (Fig. S4 in Supplemental Material [4]). The FL coefficient A increases with pressure up to ~2 GPa, suggesting strengthening electron-electron correlations, but it decreases at higher pressures. This nonmonotonic behavior may be attributed to pressure-induced microstrain or structural disorder, which could reduce correlation effects by disturbing the electronic coherence. These results highlight a complex interplay between pressure, microstructural strain, CDW formation, and scattering mechanisms in $BaFe_2Al_9$. The enhanced residual resistivity and evolving FL parameters collectively point toward Fermi surface reconstruction and the critical role of lattice effects in shaping the CDW ground state under pressure.

The static magnetic susceptibility as a function of the temperature [$\chi(T)$] is shown in Fig. S5(a) in Supplemental Material [4]. $\chi(T)$ shows a sharp jump at $T_{\mathrm{CDW}} \approx 107$ K, consistent with a first-order transition and significant Fermi surface changes. A Curie-like upturn at low temperatures and Brillouin-like magnetization at 1.8 K indicate the presence of quasifree localized moments with a small saturation moment (~0.01 μ_{B}/f.u.) [Supplemental Material Fig. S5(b) [4]]. The strong jump is indicative of a discontinuous phase transition, and the associated changes in the static susceptibility of $\Delta\chi \simeq 3.4 \times 10^{-4}$ erg/(G^2 mol) indicate considerable changes of the Fermi surface at T_{CDW}.

Figure 2(a) shows the magnetization as a function of the temperature [$M(T)$] for $BaFe_2Al_9$ under pressures up to 1.40 GPa, measured during heating in a 1 T field. Figure 2(b) presents the pressure dependence of T_{CDW} determined from both cooling and heating measurements, showing a linear increase with pressure that is consistent with our resistivity results. Supplemental Material Fig. S6 [4] shows a thermal hysteresis of ~10 K (98 K cooling, 107 K heating) confirming a first-order CDW transition at ambient pressure. The magnetization remains flat from 300

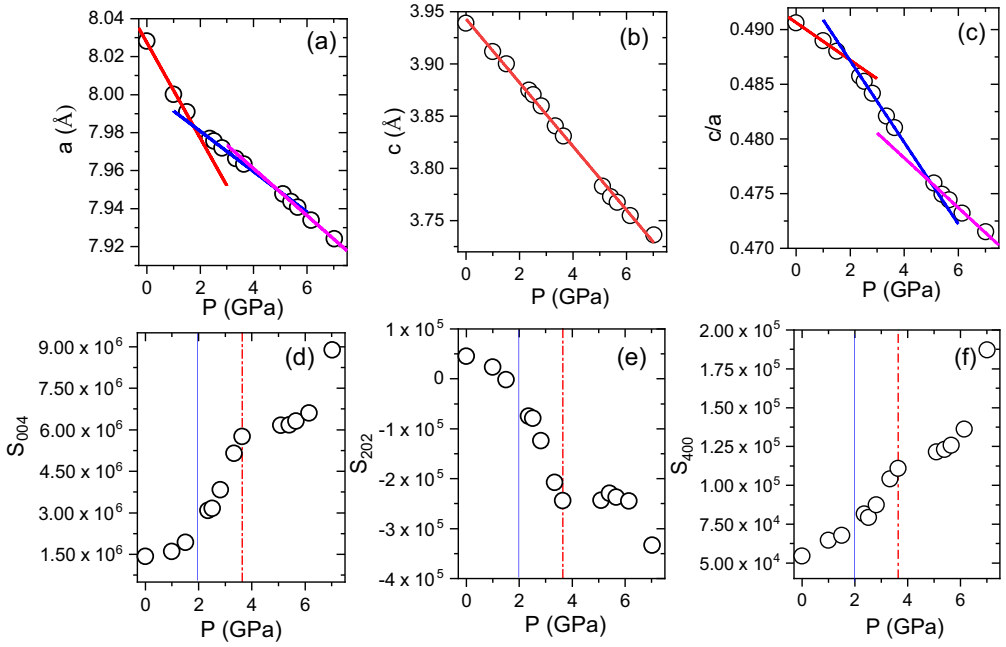

FIG. 3. Pressure evolution of the lattice parameters and anisotropic microstrain coefficients of $BaFe_2Al_9$ at room temperature. (a),(b) Lattice constants a and c versus pressure with linear fits over selected intervals. (c) The axial ratio c/a vs pressure, showing continuous compression with no symmetry-breaking discontinuity. (d)–(f) Anisotropic microstrain coefficients vs pressure, displaying a pronounced anomaly at 3.6 GPa (vertical dashed red lines). The concurrence of this microstrain anomaly with the pressure range where T_{CDW} reaches room temperature indicates a pressure-driven crossover in the character of the CDW without a first-order structural transition.

to 160 K, with a low-temperature upturn due to localized Fe moments. After releasing pressure, the data return to the initial state, indicating good hydrostatic conditions. Complementary data collected during the cooling process are shown in Supplemental Material Fig. S7 [4]. Both heating and cooling data show weaker signals, and only the onset of T_{CDW} is clearly resolved at high pressure. The differences between the T_{CDW} values obtained from the magnetization and electrical resistivity measurements result from the use of different criteria: In electrical transport, T_{CDW} is defined by the peak in the $d\rho/dT$, while in the magnetization it is identified by the initial appearance of the anomaly.

We initially anticipated a structural phase transition associated with the T_{CDW} near 3.2 GPa at 300 K, as suggested by HP $\rho(T)$. To investigate this, we performed synchrotron HP-PXRD experiments at room temperature. Figure S8 in Supplemental Material [4] presents the collected PXRD patterns of $BaFe_2Al_9$ up to ~7.0 GPa. No appearance or disappearance of diffraction peaks was observed across this pressure range, indicating the absence of a symmetry changing structural phase transition. At ambient pressure, several diffraction peaks, specifically (200)/(101), (210)/(201), (220)/(301)/(002), and the overlapping (411)/(222) are closely spaced. As pressure increases, these peaks gradually move apart, thus evidencing an anisotropic lattice compression. These peak separations are highlighted by blue arrows in Supplemental Material Fig. S8 [4]. Figures S9(a)–9(d) in Supplemental Material show Rietveld refinements of the diffraction data at selected pressures: 0, 2.52, 5.10, and 7.02 GPa. The refinements were performed using the CIF file from Ref. [5]. The refinement indeed confirms that the structural symmetry remains preserved throughout the pressure range.

Figures 3(a) and 3(b) show the pressure-dependent evolution of lattice parameters a and c. No clear first-order transition is observed near 3.2 GPa. In fact, the c axis compresses nearly linearly at -0.03 Å/GPa in the entire pressure range [Fig. 3(b)]. Instead, as indicated by the solid lines in Fig. 3(a), the a axis exhibits distinct compression rates: -0.025 Å/GPa for low pressure $0-1.51$ GPa, -0.010 Å/GPa for intermediate pressure $2.3-3.64$ GPa, and -0.012 Å/GPa for high pressure $5.1-7$ GPa. These variations are reflected also reflected well in the c/a ratio [Fig. 3(c)], which decreases at rates of -0.0017, -0.003, and -0.0028 GPa^{-1} across the same pressure ranges. Taken together, these results confirm an anisotropic lattice compression. Figure S10(a) in Supplemental Material [4] shows normalized lattice parameters emphasizing greater compressibility along c than a, evidencing a clear large axial anisotropy. The nonlinearity suggests a complex response of the lattice, and the in-plane compression may point to pressure-driven distortion or instability within the Fe-Al framework, which lies in the basal plane. Compared to the complex anisotropic response of the crystal lattice, the

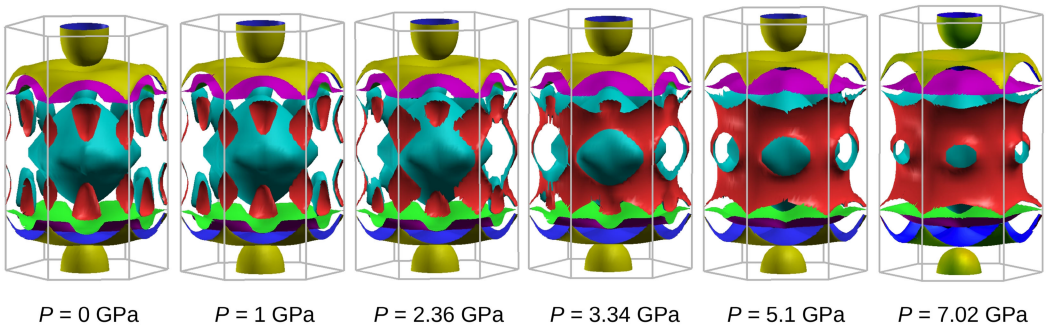

FIG. 4. FS of $BaFe_2Al_9$ at different pressures calculated using DFT taking the experimentally obtained lattice parameters (with the fractional coordinates of Al fixed to the ambient condition data).

overall unit-cell volume shows a smooth variation with pressure and is found to be well described by a second-order Birch-Murnaghan equation of state. The equation-of-state fit to the experimental data yields the bulk modulus (B_0) to be 75.0 GPa [with the $V_0 = 219.8$ Å^3; see Supplemental Material Fig. S10(b) [4]]. To have further inputs on the structure evolution of $BaFe_2Al_9$ under pressure, we employed Stephens's phenomenological model for anisotropic diffraction peak broadening [20] implemented within the Rietveld refinement framework. Because of the hexagonal symmetry of the compound (space group $P6/mmm$), the strain-induced broadening of the Bragg reflections was modeled as a function of the Miller indices hkl using the variance of the reciprocal lattice spacing $M_{hkl} = 1/d^2_{hkl}$. For hexagonal systems, this variance is given by

$$\mathrm{Var}(M_{hkl}) = \mathrm{S}_{400}(h^2 + hk + k^2)^2 + \mathrm{S}_{202}(h^2 + hk + k^2)l^2 + \mathrm{S}_{004}(l)^4.$$

Here, S_{400}, S_{202}, and S_{004} are the anisotropic strain coefficients corresponding to the in-plane, mixed, and out-of-plane strain components, respectively. These parameters were extracted from the Rietveld refinement analysis of the HP-XRD data using GSAS-II [13].

Figures 3(d)–3(f) show the calculated microstrain model parameters S_{004}, S_{202}, and S_{400} as a function of pressure as obtained from the GSAS-II Rietveld refinement analysis [13]. The data show that both S_{400} and S_{004} increase systematically with pressure, indicating enhanced microstrain along both the $a-b$ plane and the c axis. In contrast, the mixed component S_{202} decreases with pressure. Importantly, all three coefficients exhibit a clear trend change of ~3.64 GPa, closely aligning with the anomaly observed in electrical transport measurements at 3.2 GPa, where a broadened CDW transition should be reaching the ambient temperature. In fact, all the coefficients show discontinuous evolution with pressure, closely mimicking the discontinuities seen in the c/a ratio. The first discontinuity seems to be correlated to the change of the first-order- to second-order-like transition seen in $\rho(T)$. This correspondence strongly suggests a coupling between the anisotropic lattice strain and the evolution of the CDW phase under pressure. The observed increase in directional microstrain likely facilitates electronic instability and may play a critical role in stabilizing the high-pressure CDW state in $BaFe_2Al_9$.

As shown in Fig. 4, the FS of $BaFe_2Al_9$ consists of several sheets, some of which are pockets (red ones) while others are more two dimensional (yellow and magenta ones). These quasi-2D FS sheets are at the kz value which corresponds to the z component $\approx 0.3\pi/a$ of the experimentally determined ordering vector for the CDW. Because of the flat character of this FS sheet and possibility of nesting, it is natural to expect that it plays a role in the CDW emergence. In our calculations, we observe that some FS sheets change visibly under pressure, in particular, the flat CDW-related sheet and the pockets. The CDW-related FS sheet becomes notably flatter, which should enhance the FS nesting along the k_z direction and enhance the CDW, in line with the experimental observation of the increased transition temperature for the CDW phase.

For comparison, we consider also the fully optimized structures of $BaFe_2Al_9$ under pressure, which we obtained using the DFT package VASP [22]. For the optimized crystal structures, the FSs were again calculated using RSPt software, and the results are shown in Fig. S11 of Supplemental Material [4]. Contrary to the experimental structures (Fig. 4), the optimized structures do not show drastic FS changes under pressure (Supplemental Material Fig. S11 [4]) even though the structural parameters vary considerably under pressure. Optimized structures, however, deviate non-negligibly from the measured ones, which indicates some major challenges for the theory to describe this system and can be a subject of a separate study.

To address the experimentally observed decrease of conductance under pressure, we have analyzed the evolution of the electronic density of states (Supplemental Material Fig. S12 [4]) near the Fermi energy calculated using DFT in the VASP code [22]. It is well known that the electronic states in this energy range contribute the most to the electronic conductance. Our calculations show that under pressure, the

electronic states are pushed away from the Fermi energy, which reduces the amount of state that can contribute to the conductance. This might potentially explain the corresponding experimental findings; however, it should be kept in mind that many mechanisms can affect the electron transport, for example, electronic correlations or scattering on defects and phonons. An analysis of such complex phenomena is beyond the scope of this Letter, but the calculated modification of electronic states (Supplemental Material Fig. S12 [4]) in our simple model already points to the nonnegligible effect of pressure on the electronic and transport properties.

In summary, our comprehensive investigation combining resistivity, magnetization, synchrotron PXRD, and FL analysis reveals that external pressure significantly enhances and stabilizes the CDW phase in $BaFe_2Al_9$. At ambient pressure, the system exhibits a sharp, first-order CDW transition, which progressively shifts to higher temperatures and broadens with pressure, reaching ∼300 K near 3.2 GPa. This evolution is accompanied by increased residual resistivity and a decrease in the FL coefficient, signaling a pressure-induced Fermi surface reconstruction and weakening of electron-electron correlations. HP PXRD confirms the absence of any structural phase transition up to 7 GPa but reveals anisotropic lattice compression and a distinct anomaly in lattice parameters ∼3.6 GPa. Most notably, the onset of a pronounced anisotropic microstrain coincides with the pressure range where the CDW transition is most enhanced, suggesting a strong coupling between lattice fluctuations and electronic instability. Our data also suggest that the CDW transition evolves from a first-order- to a more second-order-like character under pressure. Altogether, our results establish a coherent framework: pressure-induced anisotropic strain and Fermi surface reorganization cooperatively shifting the CDW phase in $BaFe_2Al_9$ to a higher temperature, with the possibility for the stabilization of this order at room temperature for relatively lower pressure values of around 3.2 GPa. This rare example thus shows where hydrostatic pressure promotes CDW order in a three-dimensional intermetallic, which hopefully will pave the way for the realization of strain-engineered electronic phases.

Acknowledgments—The authors thank the Xpress beamline of the Elettra Sincrotrone Trieste for beamtimes (Proposal No. 20220489) and the DST government of India for financial support to execute the beamtimes. G. L. and M. H. acknowledge the support from the ARG01-0516-230179 project funded by QRDI. G. L. and M. S. gratefully acknowledge the receipt of a fellowship from the ICTP Programme for Training and Research in Italian Laboratories, Trieste, Italy. N. J. and M. A. H. acknowledge the Advanced Materials Research Lab at the University of Sharjah. S. A. wishes to thank DAE-BRNS (Mumbai) for their financial support. R. K. and L. F. C. acknowledge support by the DFG via the Heidelberg STRUCTURES Cluster (Grant No. EXC2181/1-390900948). The Swedish Research Council (Vetenskapsrådet, VR) Grants No. 2016–05980, No. 2019–05304, and No. 2024–04986, and Knut and Alice Wallenberg Foundation Grants No. 2018.0060, No. 2021.0246, and No. 2022.0108 are acknowledged (A. D. and O. E.). The Wallenberg Initiative Materials Science for Sustainability (WISE) funded by the Knut and Alice Wallenberg Foundation is also acknowledged (O. E., A. D. and V. B.). The computations/data handling were enabled by resources provided by the National Academic Infrastructure for Supercomputing in Sweden (NAISS), partially funded by the Swedish Research Council through Grant Agreement No. 2022–06725. O. E. also acknowledges support from STandUPP and eSSENCE, as well as the ERC (FASTCORR-Synergy Grant No. 854843). V. B. acknowledges support by the Swedish Research Council through Grant No. 2024-05206. K. A. Irshad acknowledges the Indian Institute of Science, Bengaluru and International Centre for Theoretical Physics, Trieste, Italy for the IISc/ICTP fellowship.

Data availability—The data that support the findings of this article are not publicly available. The data are available from the authors upon reasonable request.

[1] S. Siddique *et al.*, Phys. Rev. B **110**, 014111 (2024).
[2] G. Lingannan, B. Joseph, P. Vajeeston, C. N. Kuo, C. S. Lue, G. Kalaiselvan, P. Rajak, and S. Arumugam, Phys. Rev. B **103**, 195126 (2021).
[3] R. Sokkalingam, G. Lingannan, M. Sundaramoorthy, C. N. Kuo, C. S. Lue, A. Sonachalam, and B. Joseph, Scr. Mater. **244**, 115999 (2024).
[4] See Supplemental Material at http://link.aps.org/supplemental/10.1103/dxzf-fx8k for additional transport, magnetization, and XRD analyses under pressure and for DFT electronic structure data.
[5] W. R. Meier *et al.*, Chem. Mater. **33**, 2855 (2021).
[6] C. N. Kuo, R. Y. Huang, L. T. Wen, H. Y. Lee, C. K. Hong, Y. R. Ou, Y. K. Kuo, and C. S. Lue, Phys. Rev. B **110**, 045128 (2024).
[7] Z. Ryżyńska, T. Klimczuk, and M. J. Winiarski, J. Solid State Chem. **289**, 121509 (2020).
[8] J. Feng *et al.*, Adv. Electron. Mater. **6**, 1901427 (2020).
[9] X. Wen *et al.*, Phys. Rev. Res. **6**, 033222 (2024).
[10] G. Lingannan, B. Joseph, M. Sundaramoorthy, C. N. Kuo, C. S. Lue, and S. Arumugam, J. Phys. Condens. Matter **34**, 245601 (2022).
[11] M. Mito, J. Phys. Soc. Jpn. **76**, 182 (2007).
[12] P. Lotti, S. Milani, M. Merlini, B. Joseph, F. Alabarse, and A. Lausi, J. Synchrotron Radiat. **27**, 222 (2020).
[13] B. H. Toby and R. B. Von Dreele, J. Appl. Crystallogr. **46**, 544 (2013).
[14] J. M. Wills and B. R. Cooper, Phys. Rev. B **36**, 3809 (1987).
[15] J. M. Wills, O. Eriksson, P. Andersson, A. Delin, O. Grechnyev, and M. Alouani, *Full-Potential Electronic Structure Method* (Springer, Berlin, 2010), Vol. 167.

[16] Y. K. Cai, C. T. Zhang, T. C. Cao, J. J. Feng, Z. He, X. Z. Xing, X. B. Liu, Z. X. Shi, B. Qian, and W. Zhou, Phys. Rev. B **110**, 094516 (2024).
[17] B. Woo *et al.*, Phys. Rev. B **87**, 125121 (2013).
[18] S. Arumugam, C. Saravanan, R. Thiyagarajan, and G. Narsinga Rao, J. Magn. Magn. Mater. **507**, 166775 (2020).
[19] K. Kadowaki and S. B. Woods, Solid State Commun. **58**, 507 (1986).
[20] P. W. Stephens *et al.*, J. Appl. Crystallogr. **32**, 281 (1999).
[21] Y. Li, M. Liu, J. Li, J. Wang, J. Lai, D. He, R. Qiu, Y. Sun, X.-Q. Chen, and P. Liu, Phys. Rev. B **110**, 195118 (2024).
[22] G. Kresse and J. Furthmüller, Phys. Rev. B **54**, 11169 (1996).